Universality in the energy spectrum of medium-sized quantum dots

Alexander Odriazola,[1] Alain Delgado,[2] and Augusto González[1]
[1]*Instituto de Cibernética, Matemática y Física, Calle E 309, Vedado, Ciudad Habana, C.P. 10400, Cuba*
[2]*Centro de Aplicaciones Tecnológicas y Desarrollo Nuclear, Calle 30 No. 502, Miramar, Ciudad Habana, C.P. 11300, Cuba*
(Received 20 August 2008; revised manuscript received 28 October 2008; published 20 November 2008)

In a two-dimensional parabolic quantum dot charged with N electrons, Thomas-Fermi theory states that the ground-state energy satisfies the following nontrivial relation: $E_{gs}/(\hbar\omega) \approx N^{3/2} f_{gs}(N^{1/4}\beta)$, where the coupling constant, β, is the ratio between Coulomb and oscillator ($\hbar\omega$) characteristic energies and f_{gs} is a universal function. We perform extensive configuration-interaction calculations in order to verify that the exact energies of relatively large quantum dots approximately satisfy the above relation. In addition, we show that the number of energy levels for intraband and interband (excitonic and biexcitonic) excitations of the dot follows a simple exponential dependence on the excitation energy whose exponent, $1/\Theta$, satisfies also an approximate scaling relation *á la* Thomas-Fermi, $\Theta/(\hbar\omega) \approx N^{-\gamma} g(N^{1/4}\beta)$. We provide an analytic expression for f_{gs} based on two-point Padé approximants and two-parameter fits for the g functions.

DOI: 10.1103/PhysRevB.78.205320 PACS number(s): 73.21.La, 68.65.Hb, 73.20.Mf

I. INTRODUCTION

Thomas-Fermi theory[1–4] has proven to be a valuable tool for the qualitative understanding of atoms and molecules. In semiconductor quantum dots,[5,6] which are a kind of artificial Thomson atoms with many possibilities for fundamental research and technical applications, Thomas-Fermi theory was shown to agree qualitatively and even quantitatively with a more elaborate approach such as density-functional theory[7,8] being asymptotically exact in the limit of large electron numbers.[9]

From the computational point of view, Thomas-Fermi theory with minor corrections is able to reproduce the ground-state energy of electrons in a quadratic potential[10] at the same level of accuracy of other semiclassical or semianalytic approaches such as large-D expansions[11] or two-point Padé approximants.[12]

In the present paper, we would like to focus on a less studied aspect of Thomas-Fermi theory: the highly nontrivial scaling relations following from it. We show that the number of electrons, N, and the coupling constant, β, enter the ground-state energy in a scaled form. We perform extensive configuration-interaction calculations for quantum dots with $20 \leq N \leq 90$ in order to verify this scaling. In addition, on the basis of the numerical results, we show that similar scaling relations are valid for the number of excited states in intraband and interband excitations. In this way, a universal parametrization of the density of energy levels in quantum dots is provided.

We start with the Hamiltonian of a two-dimensional (2D) parabolic quantum dot charged with N electrons. In oscillator units, the Hamiltonian can be written as

$$\frac{H}{\hbar\omega} = \frac{1}{2}\sum_i \{p_i^2 + r_i^2\} + \beta \sum_{i<j} \frac{1}{r_{ij}}. \tag{1}$$

The only approximations made in writing Eq. (1) are the effective-mass description of electrons, the inclusion of an effective low-frequency dielectric constant, ϵ, to model the medium, and the description of confinement by means of a harmonic-oscillator potential. These approximations are very common and well sustained.[6] The coupling constant $\beta = E_{Coul}/(\hbar\omega) = e^2 m^{1/2}/(4\pi\epsilon\omega^{1/2}\hbar^{3/2})$ is the ratio of the Coulomb and harmonic-oscillator characteristic energies.

The fact that the number of electrons may enter the energy in a scaled combination with β is, however, not trivial. Let us write the Thomas-Fermi energy functional[9] for the present problem;

$$\frac{E_{TF}}{\hbar\omega} = \int d^2r \left\{ \alpha n^2 + \frac{nr^2}{2} \right\} + \beta \int\int d^2r d^2r' \frac{n(r)n(r')}{|\vec{r} - \vec{r}'|}, \tag{2}$$

where $n(r)$ is the (surface) density at point r and α is a numerical constant. The above functional should be extremized under the constraint,

$$N = \int d^2r n. \tag{3}$$

Now, it is easy to realize that we can scale r and n in such a way that the left-hand side of Eq. (3) becomes one and a factor $N^{3/2}$ is extracted from the right-hand side of Eq. (2). As a result, we get the following relation for the ground-state energy in the Thomas-Fermi approximation:

$$\frac{E_{gs}}{(\hbar\omega)} \approx N^{3/2} f_{gs}(N^{1/4}\beta). \tag{4}$$

Notice that the scaled Thomas-Fermi equations depend on a single parameter, $z = N^{1/4}\beta$, which combines in a particular way the coupling constant and the number of electrons.

II. SCALING IN THE GROUND-STATE ENERGY

We first provide an analytical expression for f_{gs} based on two-point Padé approximants[12] in the large-N limit. It shows that the scaling predicted by the Thomas-Fermi theory is quite general and compatible with true quantum effects.

Let us recall the definition of the $P_{4,3}$ Padé approximant for the ground-state energy, given in Ref. 12, which interpolates between the $\beta \to 0$ (perturbation theory) and $\beta \to \infty$ (Wigner "crystal") expansions;

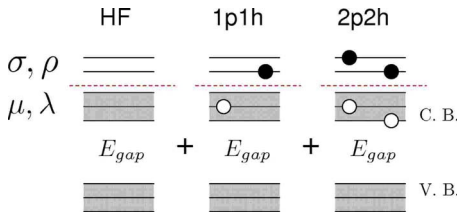

FIG. 1. (Color online) Different contributions to the ground-state wave function entering the configuration-interaction calculation.

$$P_{4,3}(\beta) = p_0 + \frac{p_1\beta + p_2\beta^{2/3}(q_2\beta^{2/3} + q_3\beta)}{1 + q_1\beta^{1/3} + q_2\beta^{2/3} + q_3\beta}. \quad (5)$$

We use the large-N asymptotic expressions for the coefficients,[12] which lead to the following estimation for the ground-state energy:

$$\frac{E_{\rm gs}}{\hbar\omega N^{3/2}} \approx \frac{2}{3} + \frac{0.698z + 1.5z^{4/3} + 2.175z^{5/3}}{1 + 2.149z^{1/3} + 1.5z^{2/3} + 2.175z}. \quad (6)$$

In order to verify the universal relation (6) we performed extensive configuration-interaction calculations for charged quantum dots. In these calculations, we follow standard procedures of quantum chemistry[13] or nuclear physics.[14]

The starting point is the Hartree-Fock solution of the problem. Then a basis of functions made up from (i) the Hartree-Fock state, $|\mathrm{HF}\rangle$, (ii) one-particle one-hole ($1p1h$) excitations, which is $|\sigma\mu\rangle = e_\sigma^\dagger e_\mu |\mathrm{HF}\rangle$, and (iii) two-particle two-hole ($2p2h$) excitations, i.e., $|\sigma\rho,\mu\lambda\rangle = e_\sigma^\dagger e_\rho^\dagger e_\mu e_\lambda |\mathrm{HF}\rangle$, is used in order to diagonalize the Hamiltonian. Notice that $\sigma < \rho$ are single-particle states above the Fermi level, and $\mu < \lambda$ are states below the Fermi level. A schematic representation is given in Fig. 1. In the Hilbert subspace with the same quantum numbers of the Hartree-Fock state, the electronic Hamiltonian takes the form,

$$H = \begin{pmatrix} E_{\rm HF} & 0 & D \\ 0 & A & B \\ D^t & B^t & C \end{pmatrix}, \quad (7)$$

where $E_{\rm HF} = \langle \mathrm{HF}|H|\mathrm{HF}\rangle$ is the Hartree-Fock energy, $A_{\sigma'\mu',\sigma\mu} = \langle \sigma'\mu'|H|\sigma\mu\rangle$ is the Tamm-Dankoff matrix, $D_{\mathrm{HF},\sigma\rho\mu\lambda} = \langle \mathrm{HF}|H|\sigma\rho,\mu\lambda\rangle$, $B_{\sigma'\mu',\sigma\rho\mu\lambda} = \langle \sigma'\mu'|H|\sigma\rho,\mu\lambda\rangle$, and $C_{\sigma'\rho'\mu'\lambda',\sigma\rho\mu\lambda} = \langle \sigma'\rho',\mu'\lambda'|H|\sigma\rho,\mu\lambda\rangle$. D^t and B^t are, respectively, the transposes of matrices D and B. Explicit matrix elements are given in Appendix A for completeness.

In sectors with quantum numbers other than the Hartree-Fock state, the first row and column of matrix (7) should be dropped.

An energy cutoff of $3\hbar\omega$ in the excitation energy is used to control the dimension of the Hamiltonian matrix. The estimated error in the ground-state energy is below 0.2%.

We computed the ground-state energy of dots with $N=20$, 30, 42, 56, 72, and 90 and confinement strengths of $\hbar\omega=6$, 12, and 18 meV. Notice that these are closed-shell quantum dots with ground-state angular momentum and spin quantum numbers $L=S=0$. GaAs parameters, $m=0.067m_0$ and $\epsilon=12.8$, were used. We performed the calculations for three-dimensional dots in which the confinement along the symmetry axis (the z axis) is modeled by a rigid-wall well of width, $L_z=25$ nm. The constant $NE_z^{(e)}$, where $E_z^{(e)} = \hbar^2\pi^2/(2mL_z^2)$, was removed from the ground-state energy. The results are depicted in Fig. 2 (dots) along with the large-N Padé estimate given by Eq. (6) (solid line). Scaling of the ground-state energy is apparent. The maximum deviations with respect to the Padé estimate are below 10% for the smallest dots with $N=20$. Notice that, for the parameters used in the calculations, the scaled variable $N^{1/4}\beta$ takes values around 1, i.e., in the transition interval from weak to strong coupling.[12] In order to test the whole interval, we use additional control cases: one of them deep in the strong-coupling regime ($N=42$ and $\hbar\omega=2$ meV) and the other in the weak-coupling region ($N=20$ and $\hbar\omega=50$ meV). They also fit the Padé estimate.

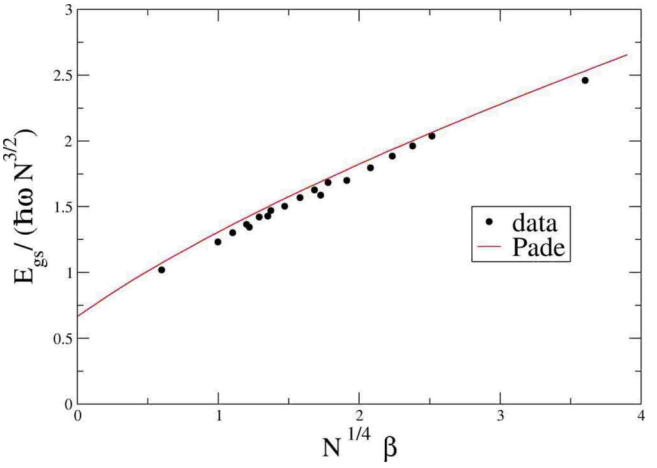

FIG. 2. (Color online) Scaling of the ground-state energy in medium-sized dots. The large-N expression for the Padé estimate [Eq. (6)] is shown as a solid line.

III. INTRABAND EXCITATIONS

We now turn to the intraband excitations. For simplicity, we consider the excited states of the closed-shell quantum dots studied above. We restrict the analysis to sectors with the same quantum numbers as the ground state, $L=S=0$, in such a way that the ground and excited states come out from the same calculation. A sample of the results is shown in Fig. 3(a) for the 42 electron dot with confinement $\hbar\omega=6$ meV. First, we notice that the excitation gap, which is $2\hbar\omega$ in the noninteracting $\beta\to 0$ limit, is renormalized by Coulomb interactions to around 6 meV, that is, 1 $\hbar\omega$. In the opposite, $\beta\to\infty$, limit, the excitation spectrum is that of a big (Wigner) molecule whose small-oscillation frequencies are independent of β.[12] The lowest of these frequencies, i.e., that one determining the gap, should go to zero for large N in order to meet the acoustic phonon of the Wigner lattice. Then, we can look for a simple interpolation formula in order to fit the numerical data for the excitation gap;

$$\frac{\Delta E_1}{\hbar\omega} = \frac{2 + a_1\beta}{1 + b_1 N^\gamma \beta}. \quad (8)$$

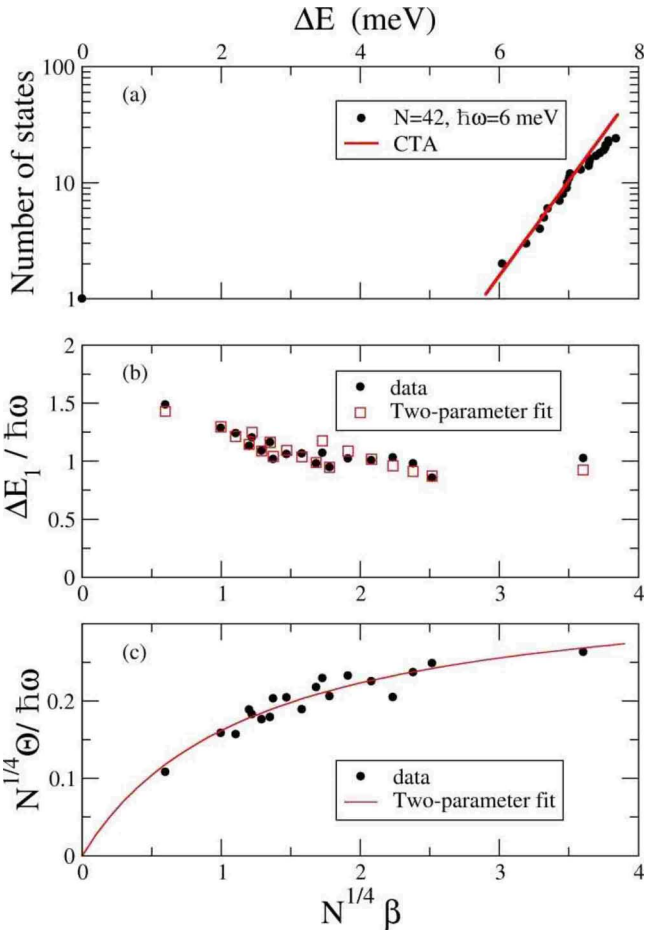

FIG. 3. (Color online) (a) The number of excited states in the 42-electron quantum dot as a function of the excitation energy. The confinement strength is $\hbar\omega=6$ meV. (b) The excitation gap to the first excited state as a function of the scaled variable $z=N^{1/4}\beta$. (c) The temperature parameter, Θ, in scaled variables. Fits in (b) and (c) correspond to Eqs. (8) and (10).

The parameter γ appears to be very close to 1/4; thus we fixed it to 1/4 and fit again the data in order to obtain a_1 and b_1. The results are shown in Fig. 3(b) as a function of $z=N^{1/4}\beta$. We stress that this is only a useful representation because ΔE_1 does not scale with z even though Fig. 3(b) shows an approximate scaling for intermediate couplings. For the parameters a_1 and b_1, we get $a_1=3.659$ and $b_1=1.878$. The result of the fit is excellent, with maximum deviations below 10%, the same as for the ground-state energy. Notice also that $N^{1/4}\Delta E_1/(\hbar\omega)$ goes to a universal value, a_1/b_1, in the strong-coupling limit, $\beta\to\infty$. Expressions similar to Eq. (8) for the gap to the first excited state should be valid in other angular momentum and spin sectors and also for the energy of collective states (spin-density and charge-density excitations).

The second point to notice in Fig. 3(a) is the exponential growth of the number of states for excitation energies above 6 meV. This simple exponential dependence on excitation energy is known in nuclear physics as the constant temperature approximation (CTA) (Ref. 15);

$$N_{\text{states}} = N_0 \exp\left(\frac{\Delta E}{\Theta}\right). \tag{9}$$

It seems to be a quite general property of the excitation spectrum of quantum systems. We verified it, for instance, in the energy spectrum of small quantum dots in strong magnetic fields.[16]

We fit the numerical data corresponding to the first 25 excited states of the quantum dots mentioned above in order to extract the "temperature" parameter, Θ, in Eq. (9). We took the first excited state as the reference of energy. The next 24 states are only a few (1–4) meV above the first excited state.

In order to deduce the universal properties of Θ let us recall the $\beta\to 0$ and $\beta\to\infty$ asymptotic regimes. In the $\beta\to\infty$ limit, we expect for Θ a behavior similar to ΔE_1, that is, $N^{1/4}\Theta/(\hbar\omega)$ should take a universal value. On the other hand, in the $\beta\to 0$ limit the excitation energies (with respect to the first excited state) are proportional to β; thus we may write a simple interpolation formula for the temperature parameter;

$$\frac{N^{1/4}\Theta}{\hbar\omega} = \frac{a_2 z}{b_2 + z}, \tag{10}$$

where $a_2=0.360$ and $b_2=1.226$. The quality of the fit is also very good as can be seen in Fig. 3(c).

IV. INTERBAND EXCITATIONS: EXCITONIC STATES

Next, we study the interband excitonic excitations of dots with $N=20$, 30, and 42 and $\hbar\omega=6$, 12, and 18 meV. The two control cases in the strong-coupling and weak-coupling regimes are also included. A basis for excitonic states in these dots is built up in the following way: (i) states with one additional electron above the Fermi level in the conduction band and a hole in the valence band, $|\sigma,\tau\rangle=e_\sigma^\dagger h_\tau^\dagger|\text{HF}\rangle$, (ii) states with two additional electrons above the Fermi level in the conduction band, a hole in the conduction band, and a hole in the valence band, $|\sigma\rho,\tau,\mu\rangle=e_\sigma^\dagger e_\rho^\dagger h_\tau^\dagger e_\mu|\text{HF}\rangle$. Details of the computational scheme in the present case can be found in Ref. 17. The Hartree-Fock single-particle states for holes are obtained from the Kohn-Luttinger Hamiltonian in the presence of the electronic background. In our model calculations, the oscillator lengths for electrons, heavy holes, and light holes are equal. Kohn-Luttinger parameters for GaAs are used.[18] With a cutoff in the excitation energy of $3\hbar\omega$, the basis dimension is reduced to around 5000.

We show in Fig. 4(a) a typical spectrum of excitonic excitations, corresponding to a dot with $N=42$ and $\hbar\omega=18$ meV. The states are characterized by the total angular momentum, $\mathcal{F}=L_e+L_h-M_h=-3/2$, and total electronic spin projections, $S=1/2$. L_e and L_h are orbital angular momenta of electrons and holes, respectively, and M is the band momentum of holes along the z axis. In Fig. 4(a), the x-axis excitation energies are measured with respect to the first excitonic state. The lowest 40 states shown in the figure follow two different CTA fits, corresponding to $\Delta E<12$ meV and

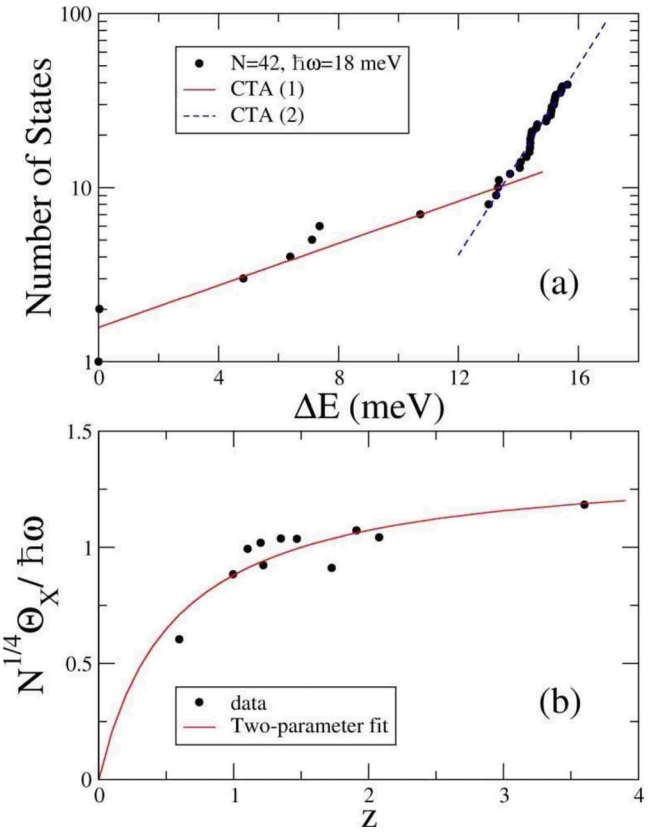

FIG. 4. (Color online) (a) The interband (excitonic) excitations in the quantum dot with 42 electrons and $\hbar\omega=18$ meV. In the x axis the reference energy is the first excitonic state. (b) Scaling of the temperature parameter for the lowest-energy excitonic states.

$12<\Delta E<16$ meV. The discontinuity in the slope seems to be a quite general fact[16] related to different mechanisms of formation of the states.

We use the lowest ten states in order to find a temperature parameter in the studied dots and a law such as Eq. (10) to fit the data. The found parameters are: $a_3=1.373$ and $b_3=0.559$. It is remarkable that the fit performs very good, as shown in Fig. 4(b), signaling that the electronic background determines global properties of the excitonic excitation spectrum. Unlike the intraband excitations, however, we expect the parameters a_3 and b_3 to depend weakly on the dot material (GaAs in this case) because of the Kohn-Luttinger Hamiltonian entering the calculations. We shall test in the future to what extent this happens.

V. INTERBAND EXCITATIONS: BIEXCITONIC STATES

Finally, let us consider the interband biexcitonic excitations in our medium-sized dots. The basis functions for the configuration-interaction calculations contains two additional electrons above the Fermi level in the conduction band and two holes in the valence band, $|\sigma\rho,\tau\eta\rangle=e^{\dagger}_{\sigma}e^{\dagger}_{\rho}h^{\dagger}_{\tau}h^{\dagger}_{\eta}|\mathrm{HF}\rangle$, with $\sigma<\rho$ and $\tau<\eta$. A schematic representation is given in Fig. 5. In Appendix B, we give explicit expressions for the Hamiltonian matrix elements.

With a cutoff in the excitation energy of $2\hbar\omega$, the Hamiltonian matrix has dimension around 3000.

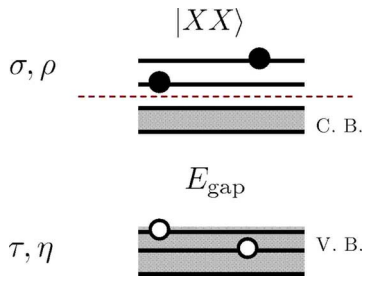

FIG. 5. (Color online) Structure of the biexcitonic wave function in the configuration-interaction calculations.

We draw in Fig. 6(a) the spectrum of biexcitonic excitations in the dot with 42 electrons and $\hbar\omega=6$ meV. The quantum numbers of the states shown in the figure are $\mathcal{F}=0$ and $S=0$. We see that in a single CTA fit we may comprise the first 35 states. These first states are to be used in the determination of the temperature parameter.

The scaling of Θ_{xx} is shown in the lower panel of Fig. 6. Notice the power of N, which is now 1/2 instead of 1/4. We verified that by taking this power, the dispersion of points is reduced notably. Thus, we fit the data with the formula,

$$\frac{N^{1/2}\Theta_{xx}}{\hbar\omega}=\frac{a_4 z}{b_4+z}, \tag{11}$$

where $a_4=3.230$ and $b_4=5.503$. The quality of the fit is very good. The same comment about the dependence of the pa-

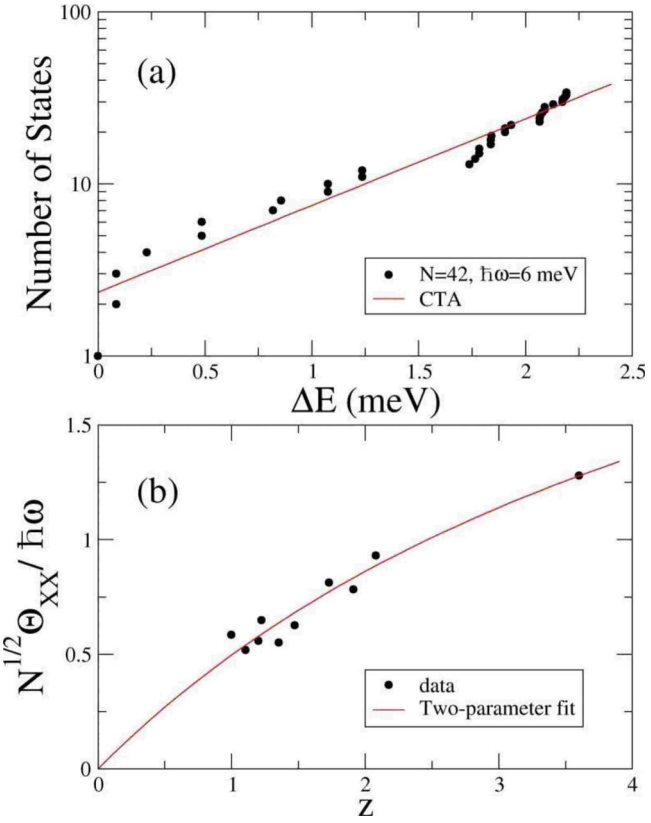

FIG. 6. (Color online) (a) The interband (biexcitonic) excitations in the quantum dot with 42 electrons and $\hbar\omega=6$ meV. In the x axis the reference energy is the first biexcitonic state. (b) Scaling of the temperature parameter for the biexcitonic excitations.

rameters on the dot material, made above for the excitonic states, applies in the present situation.

VI. CONCLUSIONS

In conclusion, we have performed extensive configuration-interaction calculations for medium-sized quantum dots in order to verify universal relations for the ground-state energy and the intraband and interband (excitonic and biexcitonic) excitation spectra. The coefficients in the right-hand side of Eqs. (6), (8), and (10) do not depend even on the material the dots are made of. On the other hand, the coefficients a_3, b_3, a_4, and b_4, we believe, are specific for GaAs but independent of N and $\hbar\omega$.

The work can be extended in many directions. We may try to parametrize in a universal way the correlation energy, the excitonic and biexcitonic binding energies, the excitation gaps to different angular momentum and spin sectors, the energy of collective (plasmonic) excitations, etc. On the other hand, more efforts toward the understanding of the empirical relations obtained for the Θ parameters are needed. Research along these lines is in progress.

ACKNOWLEDGMENTS

Part of this work was performed using the computing facilities of the Abdus Salam ICTP, Trieste, Italy. The authors acknowledge support from the Caribbean Network for Quantum Mechanics, Particles, and Fields (ICTP) and from the Programa Nacional de Ciencias Básicas (Cuba).

APPENDIX A: EXPLICIT MATRIX ELEMENTS FOR INTRABAND EXCITATIONS

In Eq. (7), E_{HF} is the Hartree-Fock total energy,[14]

$$E_{\mathrm{HF}} = \frac{1}{2}\sum_{\mu\le\mu_F}\left\{\varepsilon_\mu^{(e)} + \sum_{k,l,S_z}|R_{klS_z}^{(\mu)}|^2\varepsilon_{kls_z}^{(0)}\right\}, \tag{A1}$$

where μ_F is the Fermi level, $\varepsilon_\mu^{(e)}$ is the Hartree-Fock energy of the electron state μ, $\varepsilon_{klS_z}^{(0)}$ is the energy of 2D oscillator states characterized by the quantum numbers k (radial number), l (angular momentum), and S_z (spin projection). That is,

$$\varepsilon_{kls_z}^{(0)} = E_z^{(e)} + \hbar\omega(2k + |l| + 1). \tag{A2}$$

The state μ is expanded in oscillator states as follows:

$$|\mu\rangle = \sum_{k,l,S_z} R_{k,l,S_z}^{(\mu)}|k,l,S_z\rangle. \tag{A3}$$

In the studied closed-shell dots, l and S_z are good quantum numbers of $|\mu\rangle$ and the above sum run only over k.

On the other hand, in Eq. (7), A is the Tamm-Dankoff matrix,[14]

$$A_{\sigma'\mu',\sigma\mu} = (E_{\mathrm{HF}} + \varepsilon_\sigma^{(e)} - \varepsilon_\mu^{(e)})\delta_{\sigma\sigma'}\delta_{\mu\mu'} + \beta\langle\sigma',\mu|\frac{1}{r_{ee}}|\widetilde{\mu',\sigma}\rangle, \tag{A4}$$

where the antisymmetrized Coulomb matrix elements are defined as

$$\langle\sigma',\mu|\frac{1}{r_{ee}}|\widetilde{\mu',\sigma}\rangle = \langle\sigma',\mu|\frac{1}{r_{ee}}|\mu',\sigma\rangle - \langle\sigma',\mu|\frac{1}{r_{ee}}|\sigma,\mu'\rangle. \tag{A5}$$

Coulomb matrix elements $\langle\sigma',\mu|1/r_{ee}|\mu',\sigma\rangle$ are computed in terms of matrix elements among oscillator states by using expansion (A3).

Finally, matrices D, B, and C are explicitly written as

$$D_{\mathrm{HF},\sigma\rho\mu\lambda} = \beta\langle\mu,\lambda|\frac{1}{r_{ee}}|\widetilde{\rho,\sigma}\rangle, \tag{A6}$$

$$B_{\sigma'\mu',\sigma\rho\mu\lambda} = \beta\Bigg\{\langle\mu,\lambda|\frac{1}{r_{ee}}|\widetilde{\mu',\rho}\rangle\delta_{\sigma\sigma'} + \langle\mu,\lambda|\frac{1}{r_{ee}}|\widetilde{\sigma,\mu'}\rangle\delta_{\rho\sigma'} + \langle\sigma',\lambda|\frac{1}{r_{ee}}|\widetilde{\rho,\sigma}\rangle\delta_{\mu\mu'} + \langle\sigma',\mu|\frac{1}{r_{ee}}|\widetilde{\sigma,\rho}\rangle\delta_{\lambda\mu'}\Bigg\}, \tag{A7}$$

$$\begin{aligned}C_{\sigma'\rho'\mu'\lambda',\sigma\rho\mu\lambda} = {} & (E_{\mathrm{HF}} + \varepsilon_\sigma^{(e)} + \varepsilon_\rho^{(e)} - \varepsilon_\mu^{(e)} - \varepsilon_\lambda^{(e)})\delta_{\sigma\sigma'}\delta_{\rho\rho'}\delta_{\mu\mu'}\delta_{\lambda\lambda'} + \beta\Bigg\{\langle\mu,\lambda|\frac{1}{r_{ee}}|\widetilde{\mu',\lambda'}\rangle\delta_{\sigma\sigma'}\delta_{\rho\rho'} + \langle\rho',\lambda|\frac{1}{r_{ee}}|\widetilde{\lambda',\rho}\rangle\delta_{\sigma\sigma'}\delta_{\mu\mu'} \\ & + \langle\rho',\mu|\frac{1}{r_{ee}}|\widetilde{\rho,\lambda'}\rangle\delta_{\sigma\sigma'}\delta_{\lambda\mu'} + \langle\rho',\lambda|\frac{1}{r_{ee}}|\widetilde{\rho,\mu'}\rangle\delta_{\sigma\sigma'}\delta_{\mu\lambda'} + \langle\rho',\mu|\frac{1}{r_{ee}}|\widetilde{\mu',\rho}\rangle\delta_{\sigma\sigma'}\delta_{\lambda\lambda'} + \langle\rho',\lambda|\frac{1}{r_{ee}}|\widetilde{\sigma,\lambda'}\rangle\delta_{\mu\mu'}\delta_{\rho\sigma'} \\ & + \langle\sigma',\lambda|\frac{1}{r_{ee}}|\widetilde{\rho,\lambda'}\rangle\delta_{\mu\mu'}\delta_{\sigma\rho'} + \langle\sigma',\lambda|\frac{1}{r_{ee}}|\widetilde{\lambda',\sigma}\rangle\delta_{\mu\mu'}\delta_{\rho\rho'} + \langle\rho',\sigma'|\frac{1}{r_{ee}}|\widetilde{\rho,\sigma}\rangle\delta_{\mu\mu'}\delta_{\lambda\lambda'} + \langle\rho',\mu|\frac{1}{r_{ee}}|\widetilde{\lambda',\sigma}\rangle\delta_{\lambda\mu'}\delta_{\rho\sigma'} \\ & + \langle\sigma',\mu|\frac{1}{r_{ee}}|\widetilde{\lambda',\rho}\rangle\delta_{\lambda\mu'}\delta_{\sigma\rho'} + \langle\sigma',\mu|\frac{1}{r_{ee}}|\widetilde{\sigma,\lambda'}\rangle\delta_{\lambda\mu'}\delta_{\rho\rho'} + \langle\rho',\lambda|\frac{1}{r_{ee}}|\widetilde{\mu',\sigma}\rangle\delta_{\mu\lambda'}\delta_{\rho\sigma'} + \langle\sigma',\lambda|\frac{1}{r_{ee}}|\widetilde{\sigma,\mu'}\rangle\delta_{\mu\lambda'}\delta_{\rho\rho'} \\ & + \langle\sigma',\lambda|\frac{1}{r_{ee}}|\widetilde{\mu',\rho}\rangle\delta_{\mu,\lambda'}\delta_{\sigma\rho'} + \langle\rho',\mu|\frac{1}{r_{ee}}|\widetilde{\sigma,\mu'}\rangle\delta_{\lambda\lambda'}\delta_{\rho\sigma'} + \langle\sigma',\mu|\frac{1}{r_{ee}}|\widetilde{\rho,\mu'}\rangle\delta_{\lambda\lambda'}\delta_{\sigma\rho'} + \langle\sigma',\mu|\frac{1}{r_{ee}}|\widetilde{\mu',\sigma}\rangle\delta_{\lambda\lambda'}\delta_{\rho\rho'}\Bigg\}.\end{aligned} \tag{A8}$$

APPENDIX B: EXPLICIT MATRIX ELEMENTS FOR BIEXCITONIC EXCITATIONS

In the biexcitonic sector, the Hamiltonian matrix elements take the form,

$$\begin{aligned}
\langle \sigma'\rho', \tau'\eta'|H|\sigma\rho, \tau\eta\rangle = {} & (E_{\mathrm{HF}} + \varepsilon_\sigma^{(e)} + \varepsilon_\rho^{(e)} + \varepsilon_\tau^{(h)} + \varepsilon_\eta^{(h)})\delta_{\sigma\sigma'}\delta_{\rho\rho'}\delta_{\tau\tau'}\delta_{\eta\eta'} + \beta\langle\sigma', \rho'|\frac{1}{r_{ee}}|\widetilde{\sigma, \rho}\rangle\delta_{\tau\tau'}\delta_{\eta\eta'} + \beta\langle\tau', \eta'|\frac{1}{r_{hh}}|\widetilde{\tau, \eta}\rangle\delta_{\sigma\sigma'}\delta_{\rho\rho'} \\
& - \beta\Bigg\{\langle\rho', \eta'|\frac{1}{r_{eh}}|\rho, \eta\rangle\delta_{\tau\tau'}\delta_{\sigma\sigma'} - \langle\rho', \eta'|\frac{1}{r_{eh}}|\rho, \tau\rangle\delta_{\eta\tau'}\delta_{\sigma\sigma'} - \langle\rho', \tau'|\frac{1}{r_{eh}}|\rho, \eta\rangle\delta_{\tau\eta'}\delta_{\sigma\sigma'} \\
& + \langle\rho', \tau'|\frac{1}{r_{eh}}|\rho, \tau\rangle\delta_{\eta\eta'}\delta_{\sigma\sigma'} - \langle\rho', \eta'|\frac{1}{r_{eh}}|\sigma, \eta\rangle\delta_{\tau\tau'}\delta_{\rho\sigma'} + \langle\rho', \eta'|\frac{1}{r_{eh}}|\sigma, \tau\rangle\delta_{\eta\tau'}\delta_{\rho\sigma'} + \langle\rho', \tau'|\frac{1}{r_{eh}}|\sigma, \eta\rangle\delta_{\tau\eta'}\delta_{\rho\sigma'} \\
& - \langle\rho', \tau'|\frac{1}{r_{eh}}|\sigma, \tau\rangle\delta_{\eta\eta'}\delta_{\rho\sigma'} - \langle\sigma', \eta'|\frac{1}{r_{eh}}|\rho, \eta\rangle\delta_{\tau\tau'}\delta_{\sigma\rho'} + \langle\sigma', \eta'|\frac{1}{r_{eh}}|\rho, \tau\rangle\delta_{\eta\tau'}\delta_{\sigma\rho'} + \langle\sigma', \tau'|\frac{1}{r_{eh}}|\rho, \eta\rangle\delta_{\tau\eta'}\delta_{\sigma\rho'} \\
& - \langle\sigma', \tau'|\frac{1}{r_{eh}}|\rho, \tau\rangle\delta_{\eta\eta'}\delta_{\sigma\rho'} + \langle\sigma', \eta'|\frac{1}{r_{eh}}|\sigma, \eta\rangle\delta_{\tau\tau'}\delta_{\rho\rho'} - \langle\sigma', \eta'|\frac{1}{r_{eh}}|\sigma, \tau\rangle\delta_{\eta\tau'}\delta_{\rho\rho'} \\
& - \langle\sigma', \tau'|\frac{1}{r_{eh}}|\sigma, \eta\rangle\delta_{\tau\eta'}\delta_{\rho\rho'} + \langle\sigma', \tau'|\frac{1}{r_{eh}}|\sigma, \tau\rangle\delta_{\eta\eta'}\delta_{\rho\rho'} \\
& - \sum_{\alpha\leq\mu_F}\left[\langle\alpha, \eta'|\frac{1}{r_{eh}}|\alpha, \eta\rangle\delta_{\tau\tau'} - \langle\alpha, \eta'|\frac{1}{r_{eh}}|\alpha, \tau\rangle\delta_{\eta\tau'} - \langle\alpha, \tau'|\frac{1}{r_{eh}}|\alpha, \eta\rangle\delta_{\tau\eta'} + \langle\alpha, \tau'|\frac{1}{r_{eh}}|\alpha, \tau\rangle\delta_{\eta\eta'}\right]\delta_{\sigma\sigma'}\delta_{\rho\rho'}\Bigg\}.
\end{aligned} \tag{B1}$$

The total Hamiltonian, H, in addition to the terms of Eq. (1), now includes the single-particle energy of holes, electron-hole, and hole-hole interactions. The Hartree-Fock electron and hole states should be expanded in oscillator functions when Coulomb matrix elements are to be computed. For hole states, coming from a Kohn-Luttinger Hartree-Fock problem, we have the expansion,

$$|\tau\rangle = \sum_{k,l,m,k_z} R^{(\tau)}_{k,l,m,k_z}|k, l, m, k_z\rangle, \tag{B2}$$

where k and l are oscillator quantum numbers, $m = \pm 3/2, \pm 1/2$ is the hole (band) angular momentum projection, and $k_z = 1, \ldots, 6$ labels the subband states in the well. The relatively large number of terms entering expansion (B2) makes the calculation of Coulomb matrix elements for holes lengthy.

[1] L. H. Thomas, Proc. Cambridge Philos. Soc. **23**, 542 (1927); E. Fermi, Rend. Accad. Naz. Lincei **6**, 602 (1927).
[2] D. A. Kirzhnits, Yu. E. Lozovik, and G. V. Shpatakovskaya, Sov. Phys. Usp. **18**, 649 (1975).
[3] E. H. Lieb, Rev. Mod. Phys. **53**, 603 (1981).
[4] L. Spruch, Rev. Mod. Phys. **63**, 151 (1991).
[5] L. Kouwenhoven and C. Marcus, Phys. World **11**(6), 35 (1998).
[6] L. Jacak, P. Hawrylak, and A. Wojs, *Quantum Dots* (Springer-Verlag, Berlin, 1998).
[7] Ll. Serra and A. Puente, Eur. Phys. J. D **14**, 77 (2001).
[8] D. Ullmo, H. Jiang, W. Yang, and H. U. Baranger, Phys. Rev. B **70**, 205309 (2004).
[9] E. H. Lieb, J. P. Solovej, and J. Yngvason, Phys. Rev. B **51**, 10646 (1995).
[10] A. Gonzalez and R. Gonzalez, Sov. Phys. Lebedev. Inst. Rep. **3**, 36 (1990).
[11] A. Belov, Yu. E. Lozovik, and A. Gonzalez, Phys. Lett. A **142**, 389 (1989).
[12] A. Gonzalez, B. Partoens, and F. M. Peeters, Phys. Rev. B **56**, 15740 (1997).
[13] C. J. Cramer, *Essentials of Computational Chemistry: Theories and Models* (Wiley, Chichester, 2006).
[14] P. Ring and P. Schuck, *The Nuclear Many-Body Problem* (Springer-Verlag, New-York, 1980).
[15] T. Ericson, Adv. Phys. **9**, 425 (1960); A. Gilbert and A. G. W. Cameron, Can. J. Phys. **43**, 1446 (1965).
[16] A. Gonzalez and R. Capote, Phys. Rev. B **66**, 113311 (2002).
[17] A. Odriazola, A. Delgado, and A. Gonzalez, Phys. Rev. B **78**, 035329 (2008).
[18] *Physics of Group IV Elements and III-V Compounds*, edited by O. Madelung, H. Weiss, and M. Schultz, Landolt-Börnstein, New Series, Group III, Vol. 17, Pt. A (Springer-Verlag, Berlin, 1982).